

BI-TP 95/27
 WUE-ITP-95-017
 hep-ph/9507372

Radiative Corrections to $\gamma\gamma \rightarrow t\bar{t}$ in the Electroweak Standard Model

A. DENNER

*Institut für Theoretische Physik, Universität Würzburg
 D-97074 Würzburg, Am Hubland, Germany*

S. DITTMAIER[†]

*Theoretische Physik, Universität Bielefeld
 D-33501 Bielefeld, Postfach 100131, Germany*

M. STROBEL

*Institut für Theoretische Physik, Universität Würzburg
 D-97074 Würzburg, Am Hubland, Germany*

Abstract:

The cross-section for $\gamma\gamma \rightarrow t\bar{t}$ with arbitrary polarized photons is calculated within the electroweak Standard Model including the complete virtual and soft-photon $\mathcal{O}(\alpha)$ corrections. We present a detailed numerical discussion of the radiative corrections with particular emphasis on the purely weak corrections. These are usually of the order of 1–10% for energies up to 1 TeV. For unpolarized or equally polarized photons they reach almost 10% close to threshold. The large corrections cannot be traced back to a universal origin like the running of α or the ρ -parameter. Apart from the energy region around the Higgs resonance ($\gamma\gamma \rightarrow H^* \rightarrow t\bar{t}$) the weak corrections are widely independent of the Higgs-boson mass.

BI-TP 95/27
 WUE-ITP-95-017
 July 1995

[†]Partially supported by the Bundesministerium für Bildung und Forschung, Bonn, Germany.

1 Introduction

The recent discovery of the top quark at the Tevatron [1, 2] was a further important step in establishing the Standard Model of the electroweak interaction (SM). The experimental values for the top-quark mass $m_t = 176 \pm 8 \pm 10$ GeV from CDF[1] and $m_t = 199_{-21}^{+19} \pm 22$ GeV from DØ[2] have been found to be in very good agreement with the SM prediction of $m_t = 173_{-13}^{+12+18}$ GeV based on precision tests at LEP1 [3]. A precision measurement of the top-quark mass together with the accurate value for the W-boson mass to be expected from LEP2 will allow to derive indirect limits on the mass of the SM Higgs boson. Moreover, many properties of the top quark such as its width and its couplings still remain to be studied experimentally.

For precision measurements of the properties of the top quark, electron-positron colliders are much better suited than proton-(anti-)proton colliders [4]. The analysis of the process $e^+e^- \rightarrow t\bar{t}$ will allow to determine the top-quark mass at the level of 0.3%, the magnetic dipole moments of the top quark at the few-percent level, and even the Higgs Yukawa coupling to the top quark.

Using Compton backscattering of laser photons off high-energy electrons, a e^+e^- collider can be turned into a $\gamma\gamma$ collider [5]. This mode provides a rich variety of interesting physical processes (for a review see e.g. Ref. [6]). In particular, it allows complementary investigations of the top quark by using the reaction $\gamma\gamma \rightarrow t\bar{t}$. Similar to the process $e^+e^- \rightarrow t\bar{t}$, an accurate investigation of its threshold allows to extract m_t and α_s and even Γ_t [7]. At high energies, the corresponding cross-section is larger than the one of $e^+e^- \rightarrow t\bar{t}$. The reaction $\gamma\gamma \rightarrow t\bar{t}$ is particularly suited to study the top-quark-photon coupling [8].

At a center-of-mass energy of 500 GeV the cross-section for $\gamma\gamma \rightarrow t\bar{t}$ amounts to $\sigma \sim 0.8$ pb and thus, assuming an integrated luminosity of 10 fb^{-1} , gives rise to about 8000 events, corresponding to a statistical error of roughly 1%. At this level of experimental accuracy an investigation of the one-loop radiative corrections is in order. The one-loop QCD corrections have already been studied in Ref. [9] and found to be large. Since the top quarks can only be detected via their decay products, e.g. in $t \rightarrow bW^+$, finite-widths effects of the top quark and irreducible background contributions, e.g. $\gamma\gamma \rightarrow b\bar{b}W^+W^-$, have to be taken into account. At tree level these contributions have been investigated in Ref. [10].

As far as the electroweak one-loop corrections are concerned, so far only the Higgs-dependent corrections have been calculated [11] and the Higgs resonance contributions have been investigated [12].

In this paper we present the results of a calculation of the complete virtual and soft-photon $\mathcal{O}(\alpha)$ radiative corrections to $\gamma\gamma \rightarrow t\bar{t}$ in the SM. The calculation was carried out with help of *Mathematica* [13]. The Feynman graphs were generated and drawn by *FeynArts* [14]. We performed two independent calculations, one using *FeynCalc* [15] and one using an independent package for loop calculations. As the analytical result is very lengthy and untransparent, we refrain from writing it down in full detail. We indicate its general structure and give analytical results only for the most important $\mathcal{O}(\alpha)$ corrections. We discuss in particular the fermion-loop corrections, the leading effects from light fermions, the Coulomb singularity, the Higgs resonance, and the heavy-Higgs effects.

In the discussion of the numerical results of course the complete corrections are included. While we have calculated these corrections for arbitrary polarized photons and top quarks, we restrict the presentation to unpolarized top quarks in this paper.

The paper is organized as follows: The notation and conventions are given in Section 2. Section 3 summarizes the lowest-order results. The evaluation and general features of the higher-order corrections are discussed in Section 4, the numerical results in Section 5. In the appendix we list some explicit formulae.

2 Notation and conventions

We consider the reaction

$$\gamma(k_1, \lambda_1) + \gamma(k_2, \lambda_2) \longrightarrow t(p, \sigma) + \bar{t}(\bar{p}, \bar{\sigma}), \quad (1)$$

where $\lambda_{1,2} = \pm 1$ denote the helicities of the incoming photons and $\sigma, \bar{\sigma} = \pm 1/2$ the spin orientations of the outgoing top quarks.

In the center-of-mass system (CMS) the momenta read in terms of the energy E of the incoming photons and the scattering angle θ

$$\begin{aligned} k_1^\mu &= E(1, 0, 0, -1), \\ k_2^\mu &= E(1, 0, 0, 1), \\ p^\mu &= E(1, -\beta \sin \theta, 0, -\beta \cos \theta), \\ \bar{p}^\mu &= E(1, \beta \sin \theta, 0, \beta \cos \theta), \end{aligned} \quad (2)$$

where $\beta = \sqrt{1 - m_t^2/E^2}$ is the velocity of the top quarks in the CMS. The Mandelstam variables are given by

$$\begin{aligned} s &= (k_1 + k_2)^2 = (p + \bar{p})^2 = 4E^2, \\ t &= (k_1 - p)^2 = (k_2 - \bar{p})^2 = m_t^2 - \frac{s}{2}(1 - \beta \cos \theta), \\ u &= (k_1 - \bar{p})^2 = (k_2 - p)^2 = m_t^2 - \frac{s}{2}(1 + \beta \cos \theta). \end{aligned} \quad (3)$$

In order to calculate polarized cross-sections, we introduce explicit polarization vectors for the photons as follows

$$\begin{aligned} \varepsilon_1^\mu(k_1, \lambda_1 = \pm 1) &= -\frac{1}{\sqrt{2}}(0, 1, \mp i, 0), \\ \varepsilon_2^\mu(k_2, \lambda_2 = \pm 1) &= \frac{1}{\sqrt{2}}(0, 1, \pm i, 0). \end{aligned} \quad (4)$$

The scattering amplitude of $\gamma\gamma \rightarrow t\bar{t}$ obeys Bose symmetry with respect to the incoming photons and—neglecting quark mixing—also CP symmetry. Consequently, the helicity amplitudes $\mathcal{M}_{\lambda_1\lambda_2\sigma\bar{\sigma}}$ are related by

$$\begin{aligned} \mathcal{M}_{\lambda_1\lambda_2\sigma\bar{\sigma}}(s, t, u) &= \mathcal{M}_{\lambda_2\lambda_1\sigma\bar{\sigma}}(s, u, t) && \text{(Bose)}, \\ \mathcal{M}_{\lambda_1\lambda_2\sigma\bar{\sigma}}(s, t, u) &= \mathcal{M}_{-\lambda_1-\lambda_2-\bar{\sigma}-\sigma}(s, u, t) && \text{(CP)}, \\ \mathcal{M}_{\lambda_1\lambda_2\sigma\bar{\sigma}}(s, t, u) &= \mathcal{M}_{-\lambda_2-\lambda_1-\bar{\sigma}-\sigma}(s, t, u) && \text{(Bose + CP)}. \end{aligned} \quad (5)$$

In the following we restrict ourselves to unpolarized top quarks. In this case, Bose and CP symmetry imply for the differential cross-sections ($d\sigma^{\lambda_1\lambda_2}/d\Omega$)

$$\begin{aligned}\left(\frac{d\sigma^{--}}{d\Omega}\right)(s, t, u) &= \left(\frac{d\sigma^{++}}{d\Omega}\right)(s, t, u) = \left(\frac{d\sigma^{\pm\pm}}{d\Omega}\right)(s, u, t), \\ \left(\frac{d\sigma^{+-}}{d\Omega}\right)(s, t, u) &= \left(\frac{d\sigma^{-+}}{d\Omega}\right)(s, u, t).\end{aligned}\quad (6)$$

This means that the cross-sections for equally polarized photons ($\pm\pm$) are equal and forward-backward-symmetric, and the ones for oppositely polarized photons ($\pm\mp$) transform into each other via $\cos\theta \rightarrow -\cos\theta$.

In lowest order $\gamma\gamma \rightarrow t\bar{t}$ is a pure QED process and therefore invariant under parity P. Hence, Born amplitudes and Born cross-sections obey the additional relations

$$\mathcal{M}_{\text{Born}, \lambda_1 \lambda_2 \sigma \bar{\sigma}}(s, t, u) = \mathcal{M}_{\text{Born}, -\lambda_1 -\lambda_2 -\sigma -\bar{\sigma}}(s, t, u) \quad (\text{P}), \quad (7)$$

and

$$\left(\frac{d\sigma_{\text{Born}}^{+-}}{d\Omega}\right)(s, t, u) = \left(\frac{d\sigma_{\text{Born}}^{-+}}{d\Omega}\right)(s, t, u), \quad (8)$$

respectively.

The scattering amplitude \mathcal{M} can be decomposed into invariant functions $F_i^{\{\text{V}, \text{A}\}, t}$ and standard matrix elements (SME) $\mathcal{M}_i^{\{\text{V}, \text{A}\}, t}$, which contain the whole information about the photon polarizations

$$\mathcal{M} = \sum_i F_i^{\text{V}} \mathcal{M}_i^{\text{V}} + \sum_i F_i^{\text{A}} \mathcal{M}_i^{\text{A}}. \quad (9)$$

Assuming CP invariance and following Ref. [16], the SME can be chosen as

$$\begin{aligned}\mathcal{M}_1^{\{\text{V}, \text{A}\}, t} &= \bar{u}(p) \not{\epsilon}_1 (\not{p} - \not{k}_2) \not{\epsilon}_2 \{1, \gamma_5\} v(\bar{p}), \\ \mathcal{M}_2^{\{\text{V}, \text{A}\}, t} &= \bar{u}(p) (\not{k}_1 - \not{k}_2) \{1, \gamma_5\} v(\bar{p}) (\varepsilon_1 \cdot \varepsilon_2), \\ \mathcal{M}_3^{\{\text{V}, \text{A}\}, t} &= \bar{u}(p) [\not{\epsilon}_1 (\varepsilon_2 k_1) - \not{\epsilon}_2 (\varepsilon_1 k_2)] \{1, \gamma_5\} v(\bar{p}), \\ \mathcal{M}_4^{\{\text{V}, \text{A}\}, t} &= \bar{u}(p) [\not{\epsilon}_1 (\varepsilon_2 \bar{p}) - \not{\epsilon}_2 (\varepsilon_1 p)] \{1, \gamma_5\} v(\bar{p}), \\ \mathcal{M}_5^{\{\text{V}, \text{A}\}, t} &= \bar{u}(p) (\not{k}_1 - \not{k}_2) \{1, \gamma_5\} v(\bar{p}) (\varepsilon_1 \cdot k_2) (\varepsilon_2 \cdot k_1), \\ \mathcal{M}_6^{\{\text{V}, \text{A}\}, t} &= \bar{u}(p) (\not{k}_1 - \not{k}_2) \{1, \gamma_5\} v(\bar{p}) (\varepsilon_1 \cdot p) (\varepsilon_2 \cdot \bar{p}), \\ \mathcal{M}_7^{\{\text{V}, \text{A}\}, t} &= \bar{u}(p) (\not{k}_1 - \not{k}_2) \{1, \gamma_5\} v(\bar{p}) [(\varepsilon_1 \cdot k_2) (\varepsilon_2 \cdot \bar{p}) + (\varepsilon_1 \cdot p) (\varepsilon_2 \cdot k_1)], \\ \mathcal{M}_{11}^{\text{V}, t} &= m_t \bar{u}(p) \not{\epsilon}_1 \not{\epsilon}_2 v(\bar{p}), \\ \mathcal{M}_{12}^{\text{V}, t} &= m_t \bar{u}(p) v(\bar{p}) (\varepsilon_1 \cdot \varepsilon_2), \\ \mathcal{M}_{13}^{\{\text{V}, \text{A}\}, t} &= m_t \bar{u}(p) [\not{\epsilon}_1 \not{k}_1 (\varepsilon_2 k_1) \pm \not{k}_2 \not{\epsilon}_2 (\varepsilon_1 k_2)] \{1, \gamma_5\} v(\bar{p}), \\ \mathcal{M}_{14}^{\{\text{V}, \text{A}\}, t} &= m_t \bar{u}(p) [\not{\epsilon}_1 \not{k}_1 (\varepsilon_2 \bar{p}) \pm \not{k}_2 \not{\epsilon}_2 (\varepsilon_1 p)] \{1, \gamma_5\} v(\bar{p}), \\ \mathcal{M}_{15}^{\text{V}, t} &= m_t \bar{u}(p) v(\bar{p}) (\varepsilon_1 \cdot k_2) (\varepsilon_2 \cdot k_1), \\ \mathcal{M}_{16}^{\text{V}, t} &= m_t \bar{u}(p) v(\bar{p}) (\varepsilon_1 \cdot p) (\varepsilon_2 \cdot \bar{p}), \\ \mathcal{M}_{17}^{\{\text{V}, \text{A}\}, t} &= m_t \bar{u}(p) \{1, \gamma_5\} v(\bar{p}) [(\varepsilon_1 \cdot k_2) (\varepsilon_2 \cdot \bar{p}) \pm (\varepsilon_1 \cdot p) (\varepsilon_2 \cdot k_1)].\end{aligned}\quad (10)$$

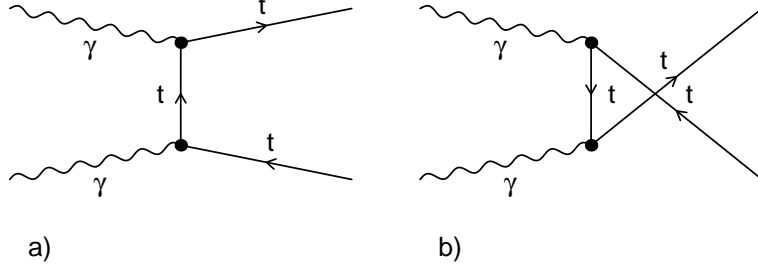


Figure 1: Lowest-order diagrams for $\gamma\gamma \rightarrow t\bar{t}$

Our choice of photon polarization vectors (4) implies

$$\varepsilon_i k_j = 0, \quad i, j = 1, 2, \quad (11)$$

and thus the SME $\mathcal{M}_{3,5,7,13,15,17}^{\{V,A\},t}$ vanish. While the SME defined in (10) are independent in D dimensions, in four dimensions the following relations hold for the non-vanishing SME

$$\begin{aligned} 0 &= (t - u)[2\mathcal{M}_1^{V,t} + \mathcal{M}_2^{V,t} - 2\mathcal{M}_4^{V,t} - 2\mathcal{M}_{11}^{V,t}] + 2s[\mathcal{M}_{11}^{V,t} - \mathcal{M}_{12}^{V,t}], \\ 0 &= (ut - m_t^4)[2\mathcal{M}_1^{V,t} + \mathcal{M}_2^{V,t} - 2\mathcal{M}_{11}^{V,t}] - 2(t - m_t^2)(u - m_t^2)\mathcal{M}_4^{V,t} - 2s[\mathcal{M}_{14}^{V,t} - 2\mathcal{M}_{16}^{V,t}], \\ 0 &= 2\mathcal{M}_1^{A,t} + \mathcal{M}_2^{A,t} - 2\mathcal{M}_4^{A,t}. \end{aligned} \quad (12)$$

The $\mathcal{M}_i^{\{V,A\},t}$ of (10) are defined such as to obtain convenient expressions for t -channel diagrams. For u -channel diagrams it is useful to introduce a second set $\mathcal{M}_i^{\{V,A\},u}$ of SME which results from the $\mathcal{M}_i^{\{V,A\},t}$ by the interchange $(k_1, \varepsilon_1) \leftrightarrow (k_2, \varepsilon_2)$. Of course, the $\mathcal{M}_i^{\{V,A\},u}$ can be completely expressed in terms of the original set $\mathcal{M}_i^{\{V,A\},t}$.

3 Lowest-order cross-section

The two tree-level diagrams for $\gamma\gamma \rightarrow t\bar{t}$ are shown in Fig. 1. The corresponding amplitude is given by

$$\mathcal{M}_{\text{Born}} = 4\pi Q_t^2 \alpha \left(\frac{\mathcal{M}_{\text{Born}}^t}{t - m_t^2} + \frac{\mathcal{M}_{\text{Born}}^u}{u - m_t^2} \right) \quad (13)$$

with

$$\mathcal{M}_{\text{Born}}^{\{t,u\}} = \mathcal{M}_1^{V,\{t,u\}} - \mathcal{M}_{11}^{V,\{t,u\}}, \quad (14)$$

leading to the differential Born cross-section

$$\left(\frac{d\sigma_{\text{Born}}}{d\Omega} \right) = \sum_{\lambda_1, \lambda_2, \sigma, \bar{\sigma}} \frac{1}{4} (1 + P_1 \lambda_1) (1 + P_2 \lambda_2) \frac{N_t^C \beta}{64\pi^2 s} |\mathcal{M}_{\text{Born}}|^2, \quad (15)$$

where P_i denotes the degree of polarization of the i -th photon, and $N_t^C = 3$ represents the colour factor for the top quark.

Using the photon polarization states defined in (4) and summing over the top-quark polarizations yields

$$\begin{aligned}
\left(\frac{d\sigma_{\text{Born}}^{\text{UU}}}{d\Omega}\right) &= Q_t^4 \alpha^2 \frac{3\beta}{2s} \left[-6m_t^8 + 3m_t^4 t^2 - m_t^2 t^3 + 14m_t^4 tu - 7m_t^2 t^2 u + t^3 u \right. \\
&\quad \left. + 3m_t^4 u^2 - 7m_t^2 tu^2 - m_t^2 u^3 + tu^3 \right] / \left[(t - m_t^2)^2 (u - m_t^2)^2 \right], \\
\left(\frac{d\sigma_{\text{Born}}^{\pm\pm}}{d\Omega}\right) &= Q_t^4 \alpha^2 \frac{3\beta}{s} \frac{m_t^2 (s - 2m_t^2) s^2}{(t - m_t^2)^2 (u - m_t^2)^2}, \\
\left(\frac{d\sigma_{\text{Born}}^{\pm\mp}}{d\Omega}\right) &= Q_t^4 \alpha^2 \frac{3\beta}{s} \frac{(ut - m_t^4)(6m_t^4 - 4m_t^2 t + t^2 - 4m_t^2 u + u^2)}{(t - m_t^2)^2 (u - m_t^2)^2}. \tag{16}
\end{aligned}$$

The superscript “UU” denotes to the completely unpolarized case. Integrating over the symmetric angular range $\theta_{\text{cut}} \leq \theta \leq 180^\circ - \theta_{\text{cut}}$, we obtain the total cross-sections

$$\begin{aligned}
\sigma_{\text{Born}}^{\text{UU}} &= 12\pi Q_t^4 \alpha^2 \frac{1}{s} \left[-\tilde{\beta} - \frac{16\tilde{\beta}m_t^4}{(1 - \tilde{\beta}^2)s^2} + \frac{s^2 + 4sm_t^2 - 8m_t^4}{s^2} \ln \frac{1 + \tilde{\beta}}{1 - \tilde{\beta}} \right], \\
\sigma_{\text{Born}}^{\pm\pm} &= 48\pi Q_t^4 \alpha^2 \frac{m_t^2 (s - 2m_t^2)}{s^3} \left[\frac{2\tilde{\beta}}{1 - \tilde{\beta}^2} + \ln \frac{1 + \tilde{\beta}}{1 - \tilde{\beta}} \right], \\
\sigma_{\text{Born}}^{\pm\mp} &= 24\pi Q_t^4 \alpha^2 \frac{1}{s} \left[-\tilde{\beta} - \frac{4\tilde{\beta}m_t^2 (s + 2m_t^2)}{(1 - \tilde{\beta}^2)s^2} + \frac{s^2 + 2sm_t^2 - 4m_t^4}{s^2} \ln \frac{1 + \tilde{\beta}}{1 - \tilde{\beta}} \right], \tag{17}
\end{aligned}$$

where $\tilde{\beta} = \beta \cos \theta_{\text{cut}}$.

Figures 7 and 8 show the cross-sections integrated over two different angular ranges ($\theta_{\text{cut}} = 0^\circ, 20^\circ$) for various polarization configurations. The angular cut reduces in particular $\sigma_{\text{Born}}^{\pm\pm}$ at high energies considerably. For energies close to threshold the cross-sections for unequal photon helicities are suppressed, more precisely $\sigma_{\text{Born}}^{\pm\mp}$ vanish like β^3 for $\beta \rightarrow 0$ while $\sigma_{\text{Born}}^{\pm\pm}$ behave like β . In the high-energy limit (with fixed θ_{cut}) the cross-sections $\sigma_{\text{Born}}^{\pm\mp}$ drop like $\ln(s)/s$ and $1/s$ for $\theta_{\text{cut}} = 0$ and $\theta_{\text{cut}} \neq 0$, respectively, whereas $\sigma_{\text{Born}}^{\pm\pm}$ behave like $1/s$ and $1/s^2$ without and with finite angular cut-off, respectively.

The angular dependence of the differential cross-sections is illustrated in Fig. 9 at $\sqrt{s} = 350, 500, 1000$ GeV. The cross-sections $d\sigma_{\text{Born}}^{\pm\pm}/d\Omega$ are maximal in the forward and backward directions owing to the approximative t - and u -channel poles. These poles are cancelled in $d\sigma_{\text{Born}}^{\pm\mp}/d\Omega$ by a kinematical zero such that these cross-sections vanish in the forward and backward directions. For low energies they possess a maximum at 90° which is split into two maxima for CMS energies above $\sqrt{2(1 + \sqrt{5})}m_t \approx 2.54m_t$. For higher energies these maxima occur at $\theta[\text{rad}] \sim m_t/E$ and $\pi - m_t/E$ so that all channels become more and more peaked in the forward and backward directions.

4 Radiative corrections

4.1 Structure of the $\mathcal{O}(\alpha)$ corrections and Feynman diagrams

Using standard techniques (e.g. described in Ref. [17]), we have calculated the complete electroweak virtual and soft-photonic corrections to $\gamma\gamma \rightarrow t\bar{t}$ in $\mathcal{O}(\alpha)$ for arbitrary photon polarizations. We have performed two completely independent calculations which

agree numerically within 9–10 digits for the considered energies. The $\mathcal{O}(\alpha)$ -corrected differential cross-section takes the general form

$$\begin{aligned} \left(\frac{d\sigma}{d\Omega} \right) &= \sum_{\lambda_1, \lambda_2, \sigma, \bar{\sigma}} \frac{1}{4} (1 + P_1 \lambda_1) (1 + P_2 \lambda_2) \frac{N_t^C \beta}{64\pi^2 s} \left[|\mathcal{M}_{\text{Born}}|^2 (1 + \delta_{\text{SB}}) + 2 \text{Re} \{ \mathcal{M}_{\text{Born}}^* \delta \mathcal{M} \} \right] \\ &= \left(\frac{d\sigma_{\text{Born}}}{d\Omega} \right) (1 + \delta), \end{aligned} \quad (18)$$

where δ_{SB} denotes the soft-photon bremsstrahlung factor in $\mathcal{O}(\alpha)$, and $\delta \mathcal{M}$ the one-loop corrections to the transition amplitude. The factor δ represents the complete relative $\mathcal{O}(\alpha)$ correction. For the integrated cross-section σ , it is defined analogously

$$\sigma = \int_{\theta_{\min}}^{\theta_{\max}} d\cos\theta \int_0^{2\pi} d\phi \left(\frac{d\sigma}{d\Omega} \right) = \sigma_{\text{Born}} (1 + \delta). \quad (19)$$

In the soft-photon approximation for the bremsstrahlung process $\gamma\gamma \rightarrow t\bar{t}\gamma$ only photons with energies below the cut-off energy $\Delta E \ll E$ are included. The IR divergence is regulated by an infinitesimal photon mass λ ; it cancels against the IR divergence of the virtual corrections. The soft-photon correction leads to the following correction factor to the lowest-order cross-section

$$\begin{aligned} \delta_{\text{SB}} &= -\frac{\alpha}{\pi} \left\{ 2 \ln \frac{2\Delta E}{\lambda} + \frac{1}{\beta} \ln \left(\frac{1-\beta}{1+\beta} \right) + \frac{s-2m_t^2}{s\beta} \left[2 \ln \frac{2\Delta E}{\lambda} \ln \left(\frac{1-\beta}{1+\beta} \right) \right. \right. \\ &\quad \left. \left. - 2 \text{Li}_2 \left(\frac{1-\beta}{1+\beta} \right) + \frac{1}{2} \ln^2 \left(\frac{1-\beta}{1+\beta} \right) + \frac{\pi^2}{3} - 2 \ln \left(\frac{1-\beta}{1+\beta} \right) \ln \left(\frac{2\beta}{1+\beta} \right) \right] \right\}, \end{aligned} \quad (20)$$

which can be easily obtained from the general results of Ref. [17].

The one-loop Feynman diagrams, which form the virtual $\mathcal{O}(\alpha)$ correction $\delta \mathcal{M}$, have been calculated in 't Hooft–Feynman gauge. The calculation of $\delta \mathcal{M}$ can be split into two different steps. Firstly, one has to evaluate the interference of the SME with the Born matrix elements for fixed photon polarizations

$$M^{\lambda_1 \lambda_2, \{V,A\}, \{t,u\}}(i, j) = \sum_{\sigma, \bar{\sigma}} \mathcal{M}_i^{\{V,A\}, \{t,u\}} \times \mathcal{M}_{\text{Born}}^{j*}, \quad (21)$$

with $i = 1, \dots, 7, 11, \dots, 17$ and $j = t, u$. These quantities are listed in App. A. The corresponding expressions for unpolarized photons, which can be obtained by averaging over the photon polarizations, were already given in Ref. [16]. Note, however, that we use a different definition of the quantities $\mathcal{M}_{\text{Born}}^{\{t,u\}}$. Secondly, one has to calculate the one-loop contributions $\delta F_i^{\{V,A\}}$ to the invariant functions $F_i^{\{V,A\}}$ defined in (9). Technically the $\delta F_i^{\{V,A\}}$ are expressed in terms of one-loop tensor integrals. The amplitude is generated with *FeynArts* [14]. Its reduction to coefficients of one-loop tensor integrals is carried out in *Mathematica* [13], once using *FeynCalc* [15] once without. Following the method of Ref. [18], the tensor coefficients are recursively calculated from the scalar one-loop integrals, which are evaluated according to Ref. [19]. We have checked our numerical routines for the calculation of the scalar one-loop integrals against the package *FF* [20].

The renormalization has been carried out in the complete on-shell scheme [17], where all mass parameters represent physical masses, and all physical fields possess residues equal to one. Consequently, self-energy insertions in external legs of Feynman graphs do not contribute. We have checked that all UV singularities cancel.

The relevant one-loop diagrams are classified with respect to their topology in self-energy, vertex and box corrections. Since the analytical form of the complete virtual corrections is very complicated and untransparent, we do not give the full explicit expressions. Instead, we list all relevant one-loop Feynman graphs and discuss only the most important radiative corrections analytically.

The top-quark self-energy is the only two-point function occurring at one loop. The corresponding t -channel diagrams are shown in Fig. 2. The u -channel diagrams are obtained from those via “crossing”, i.e. by interchanging the incoming photon lines. For renormalization only the ZA -mixing energy is needed in addition.

The vertex corrections can be divided into three very different classes. Firstly, there are $At^*\bar{t}$ and $At\bar{t}^*$ vertex corrections in the t and u channel, where asterisks mark off-shell fields. The Feynman graphs for the $At^*\bar{t}$ vertex corrections are shown in Fig. 3, the $At\bar{t}^*$ vertex graphs are obtained from those by reversing the top-quark lines. The second and third type of vertex corrections concern the AAZ^*/χ^* and AAH^* couplings, respectively, with χ being the neutral would-be Goldstone boson field related to the Z boson. The (s -channel-like) diagrams are depicted in Figs. 4 and 5, and the corresponding corrections are discussed in more detail in the subsequent sections.

The irreducible one-loop diagrams, so-called boxes, are shown in Fig. 6.

4.2 Gauge-invariant subsets of Feynman diagrams

The classification of Feynman graphs according to their topology is very convenient for practical calculations, but as a matter of fact not based on physical grounds. This is due to the fact that the single vertex functions in general do not represent gauge-invariant subsets of diagrams. On the other hand, it is very desirable to decompose the complicated structure of the complete $\mathcal{O}(\alpha)$ corrections into parts which are of different physical origin and can be discussed separately. Indeed, the fact that we omit here the QCD corrections is already such a separation.

The process $\gamma\gamma \rightarrow t\bar{t}$ can also be treated in pure QED, which is part of the SM. Consequently, all QED-like diagrams, i.e. the ones with only A and t fields as virtual lines, form a gauge-invariant subset. Thus, we define the one-loop QED corrections δ_{QED} by the sum of the soft-photon correction δ_{SB} and the contribution of the photonic one-loop diagrams shown in 2.c, 3.g and 6.o, their counterparts arising from particle interchange, and the corresponding terms in the top-quark field and mass renormalization.

Since the number of fermion generations in the SM is a free parameter of the theory, each fermion generation yields a gauge-invariant subset of one-loop diagrams formed by fermionic loops. For $\gamma\gamma \rightarrow t\bar{t}$ this set is furnished by the diagrams 4.a, 4.b, 5.a, and their crossed counterparts. In the following we call these fermion-loop corrections δ_{ferm} . Actually, the fermion-loop corrections to the AAH^* vertex on the one hand and to the AAZ^*/χ^* vertices on the other hand are separately gauge-invariant. This becomes clear e.g. by inspecting the process $\gamma\gamma \rightarrow t\bar{t}$ within the gauged non-linear σ -model [21]. This model represents an $SU(2) \times U(1)$ gauge theory either, which is equivalent to the SM in

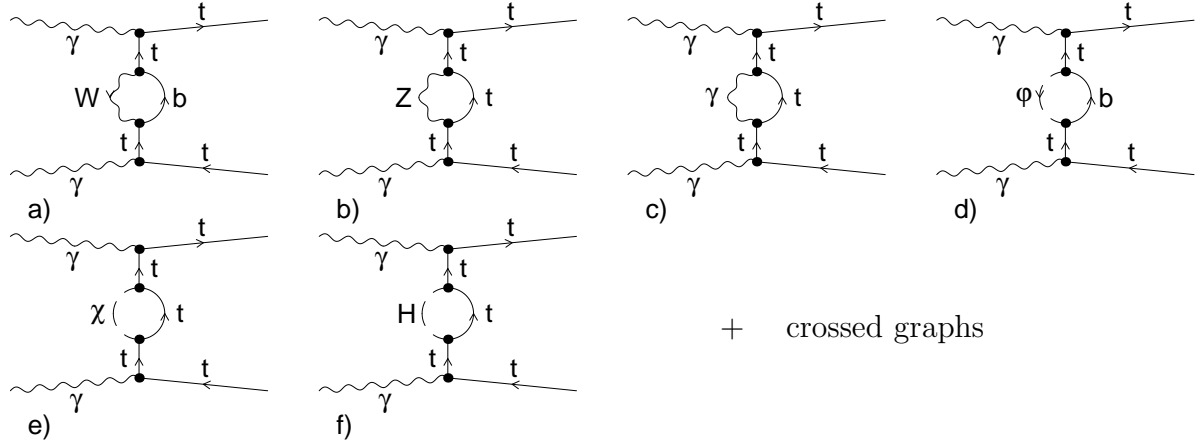


Figure 2: Top-quark self-energy diagrams

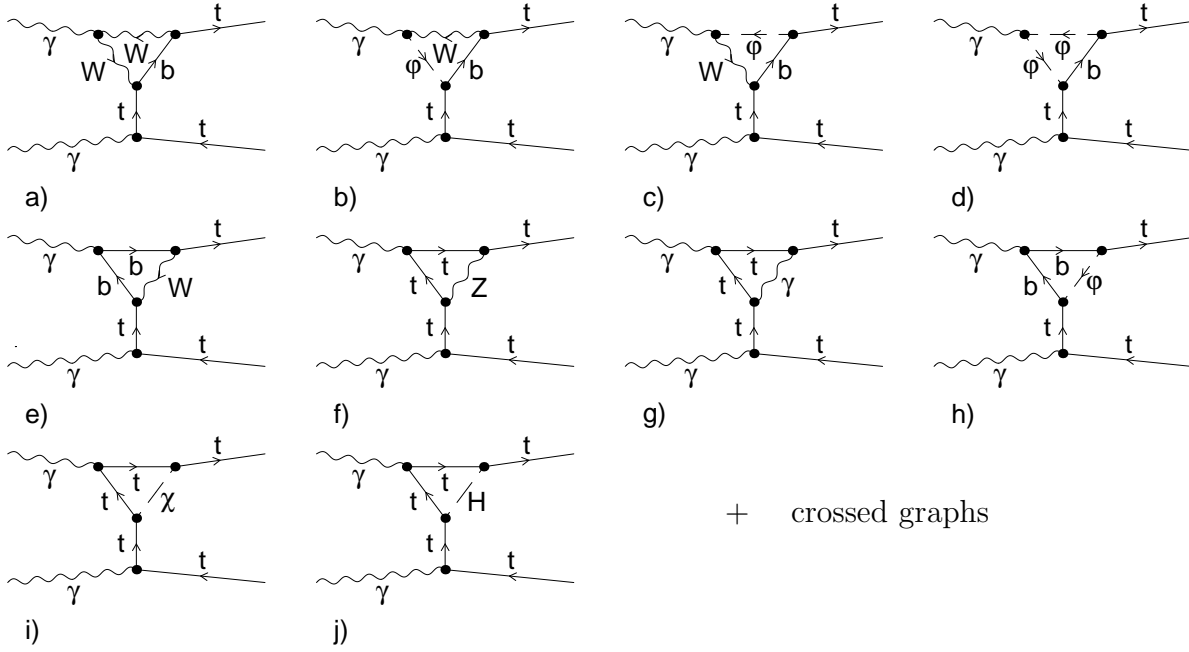


Figure 3: $At^*\bar{t}$ vertex diagrams

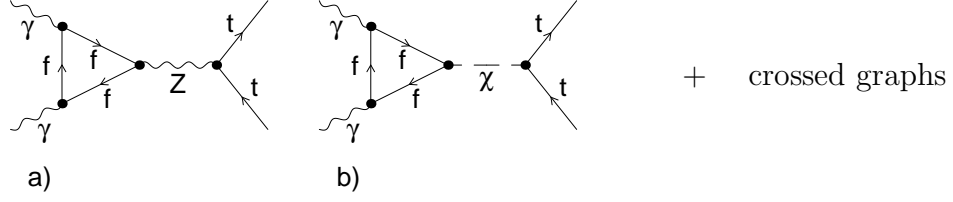


Figure 4: AAZ^* and $AA\chi^*$ vertex corrections

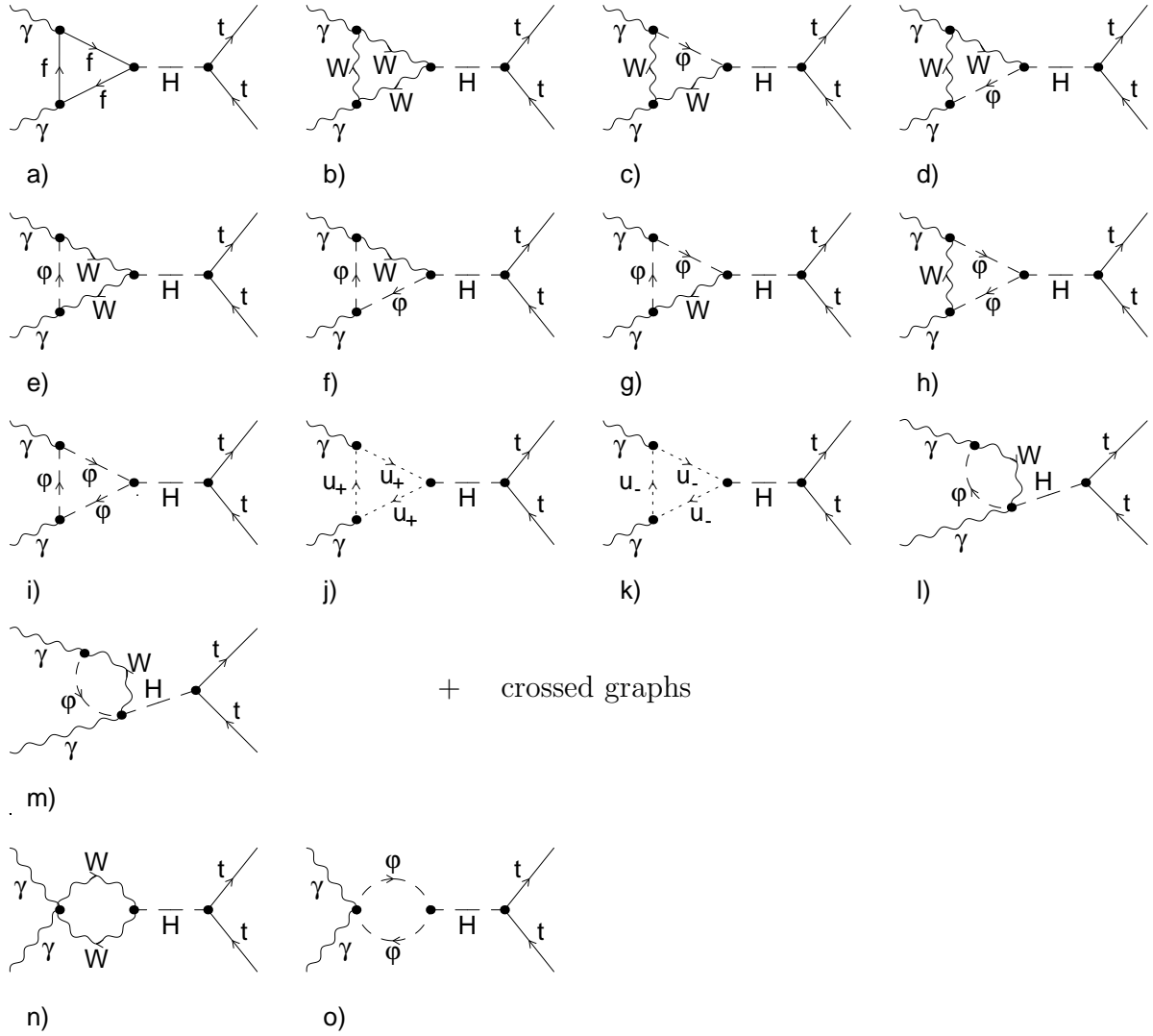


Figure 5: AAH^* vertex corrections (Graphs n,o do not possess crossed counterparts.)

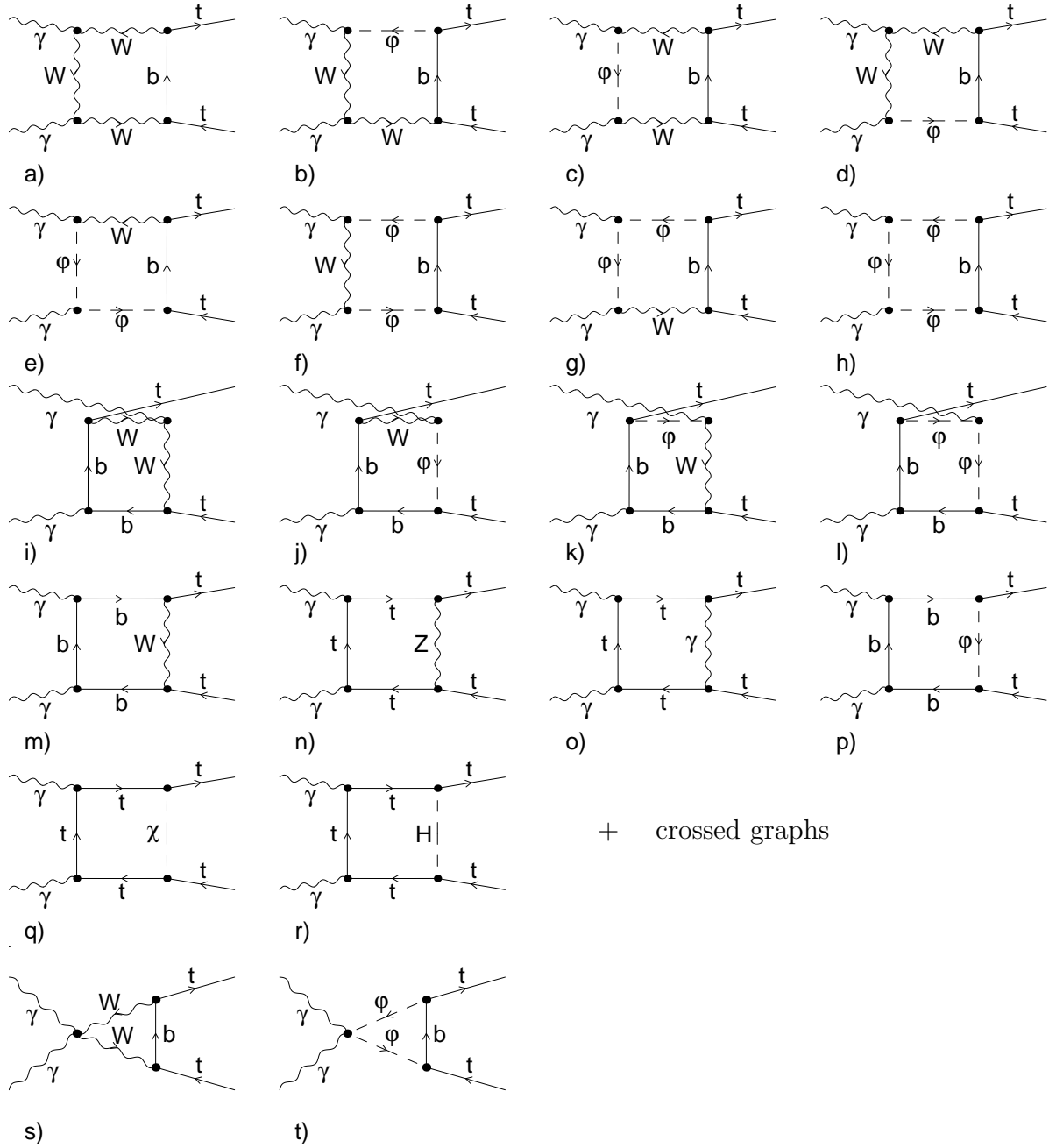


Figure 6: Box corrections (Graphs s,t do not possess crossed counterparts.)

the unitary gauge without physical Higgs boson. However, in this model without Higgs field the AAZ^*/χ^* corrections are identical with the ones in the SM.

Of course, all virtual diagrams which are not contained in δ_{QED} or δ_{ferm} form a gauge-invariant subset, too. We call the corresponding corrections “bosonic” and denote it by δ_{bos} . In summary, we have the decomposition of the $\mathcal{O}(\alpha)$ corrections δ

$$\delta = \delta_{\text{QED}} + \delta_{\text{ferm}} + \delta_{\text{bos}}. \quad (22)$$

In the following we mainly concentrate on the non-QED or “weak” corrections defined as

$$\delta_{\text{weak}} = \delta_{\text{ferm}} + \delta_{\text{bos}}. \quad (23)$$

4.3 AAZ^* and $AA\chi^*$ vertex corrections

In 't Hooft–Feynman gauge the fermion-loop contributions to the AAZ^* and $AA\chi^*$ vertices (see Fig. 4) are given by

$$\begin{aligned} \delta\mathcal{M}^{AAZ^*} &= \frac{2\alpha^2}{s_W^2 c_W^2} \frac{s}{(u-t)(s-M_Z^2)} [\mathcal{M}_{11}^{V,t} - \mathcal{M}_{12}^{V,t}] \sum_f N_f^C Q_f^2 I_{W,f}^3 m_f^2 C(s, m_f), \\ \delta\mathcal{M}^{AA\chi^*} &= -\frac{s}{M_Z^2} \delta\mathcal{M}^{AAZ^*}, \end{aligned} \quad (24)$$

where the relations (12) between the SME have been used, and $c_W = M_W/M_Z$, $s_W = \sqrt{1-c_W^2}$ denote the sine and cosine of the weak mixing angle. The sum over \sum_f runs over all (massive) fermions f with colour factor N_f^C , electric charge Q_f , third component of weak isospin $I_{W,f}^3$, and mass m_f . In (24) $C(s, m)$ denotes the scalar three-point function (see e.g. Ref. [17])

$$C(s, m) = C_0(s, 0, 0, m, m, m) = \frac{1}{2s} \ln^2 \left(\frac{r+1}{r-1} \right), \quad \text{with } r = \sqrt{1 - \frac{4m^2}{s+i\epsilon}}. \quad (25)$$

Note that the pole at $s = M_Z^2$ drops out in the gauge-invariant sum of $\delta\mathcal{M}^{AAZ^*}$ and $\delta\mathcal{M}^{AA\chi^*}$,

$$\begin{aligned} \delta\mathcal{M}^{AAZ^*+AA\chi^*} &= \delta\mathcal{M}^{AAZ^*} + \delta\mathcal{M}^{AA\chi^*} \\ &= \frac{2\alpha^2}{s_W^2 M_W^2} \frac{s}{(t-u)} [\mathcal{M}_{11}^{V,t} - \mathcal{M}_{12}^{V,t}] \sum_f N_f^C Q_f^2 I_{W,f}^3 m_f^2 C(s, m_f) \\ &= -\frac{2\alpha^2}{s_W^2 M_W^2} \lambda_1 \sqrt{s} m_t \delta_{\lambda_1 \lambda_2} \delta_{\sigma\bar{\sigma}} \sum_f N_f^C Q_f^2 I_{W,f}^3 m_f^2 C(s, m_f). \end{aligned} \quad (26)$$

Since $\delta\mathcal{M}^{AAZ^*+AA\chi^*}$ is gauge-invariant, it is equal to $\delta\mathcal{M}^{AAZ^*}$ in the unitary gauge, which has been checked explicitly.

As can be seen in (26), this correction only contributes for equally polarized photons. The top-loop contribution is enhanced by a factor $m_t^2/(s_W^2 M_W^2)$. Close to threshold an additional enhancement results from the scalar 3-point function which tends to

$$C(s, m_f) \sim -\frac{\pi^2}{2s} \quad (27)$$

such that these diagrams give rise to corrections of about 10%.

4.4 Higgs resonance

The contribution of the AAH^* vertex corrections (see Fig. 5) reads (compare Ref. [12])

$$\delta\mathcal{M}^{AAH^*} = \frac{F^H(s)}{s - M_H^2} \mathcal{M}_{12}^{V,t} = -\frac{F^H(s)}{s - M_H^2} \beta \sqrt{s} m_t \text{sgn}(\sigma) \delta_{\lambda_1 \lambda_2} \delta_{\sigma \bar{\sigma}}, \quad (28)$$

where

$$F^H(s) = \frac{\alpha^2}{2s_W^2} \left\{ -2 \sum_f N_f^C Q_f^2 \frac{m_f^2}{M_W^2} \left[2 + (4m_f^2 - s) C(s, m_f) \right] + \left[\frac{M_H^2}{M_W^2} + 6 + (M_H^2 + 12M_W^2 - 7s) C(s, M_W) \right] \right\}, \quad (29)$$

with $C(s, m)$ defined in (25). From (28) we recognize that $\delta\mathcal{M}^{AAH^*}$ vanishes unless the photons are equally polarized. While the fermionic part of $F^H(s)$ is gauge-invariant, the bosonic part depends on the gauge. Equation (29) is written down in 't Hooft–Feynman gauge. Up to a proportionality factor containing the SME, $\delta\mathcal{M}^{AAH^*}$ has the same analytical structure as the corresponding corrections to $\gamma\gamma \rightarrow W^+W^-$ [22] evaluated in 't Hooft–Feynman gauge.

For $s \rightarrow M_H^2$ the correction $\delta\mathcal{M}^{AAH^*}$ becomes resonant, i.e. finite-width effects of the Higgs boson have to be taken into account. Introducing a constant or energy-dependent width via the substitution $(s - M_H^2)^{-1} \rightarrow (s - M_H^2 + iM_H\Gamma_H)^{-1}$ clearly breaks gauge invariance. Instead, we split $\delta\mathcal{M}^{AAH^*}$ into a gauge-invariant resonant and gauge-dependent non-resonant part, and introduce a constant width only in the former,

$$\frac{F^H(s)}{s - M_H^2} \rightarrow \frac{F^H(M_H^2)}{s - M_H^2 + iM_H\Gamma_H} + \frac{F^H(s) - F^H(M_H^2)}{s - M_H^2}. \quad (30)$$

For a calculation with order $\mathcal{O}(\alpha)$ accuracy also near $s = M_H^2$, one should take into account the $\mathcal{O}(\alpha)$ corrections to the Higgs-boson width [23] and to $F^H(s)$ in the resonant contribution, i.e. for $s \sim M_H^2$. Since the Higgs resonance is not our main concern, we only take into account the lowest-order decay width determined from the imaginary part of the one-loop Higgs-boson self-energy and (29) for $F^H(M_H^2)$.

4.5 Special features of the electroweak one-loop corrections

Here we discuss some interesting peculiarities of the electroweak one-loop corrections to $\gamma\gamma \rightarrow t\bar{t}$. These are related to the fact that this process involves no light charged external particles and that the tree-level matrix elements involve only QED couplings. Similar features have been observed in the process $\gamma\gamma \rightarrow W^+W^-$ [22].

(i) Coulomb singularity

Near threshold every pair-production process of charged particles gets large photonic corrections which are due to the well-known *Coulomb singularity*. The relative correction behaves like β^{-1} , more precisely it approaches asymptotically the universal factor

$$\delta\sigma_{\text{Coul.}} = \frac{\alpha\pi}{2\beta} Q_t^2 \sigma_{\text{Born}}. \quad (31)$$

Diagrammatically this correction originates from the box diagram 6.o and its crossed counterpart and is contained in the QED part δ_{QED} of the complete $\mathcal{O}(\alpha)$ correction. The modifications of the Coulomb singularity owing to the finite top-quark width have been discussed in Ref. [24].

(ii) Leading logarithmic QED corrections

Because $\gamma\gamma \rightarrow t\bar{t}$ involves no light charged external particles, no large logarithmic corrections associated with collinear photons arise for not too high energies. Consequently, the QED corrections are of the same order as the weak corrections.

(iii) Heavy Higgs effects

In the limit $M_H \gg s, m_t$, for fixed α , M_Z , M_W , no large logarithmic corrections of the form $\ln(M_H^2/|q^2|)$ with $q^2 = s, t, u, m_t^2$ occur. In other words the $\mathcal{O}(\alpha)$ correction δ approaches a constant in the formal limit $M_H \rightarrow \infty$. The absence of $\ln M_H$ terms is associated with the fact that the one-loop correction to $\gamma\gamma \rightarrow t\bar{t}$ is UV-finite in the gauged non-linear σ -model despite of its non-renormalizability. Inspecting also the finite terms in the heavy-Higgs limit, one finds that the SM one-loop corrections for $M_H \rightarrow \infty$ exactly coincide with the ones of the gauged non-linear σ -model. This has been explicitly shown in Ref. [25], where the physical Higgs field of the SM was integrated out.

(iv) Running $\alpha(q^2)$ and ρ -parameter

Coupling constant renormalization often leads to large universal corrections entering via the running of the electromagnetic coupling $\alpha(q^2)$ or the ρ -parameter. For $\gamma\gamma \rightarrow t\bar{t}$ no such corrections exist since on-shell photons naturally couple with $\alpha(0) = \alpha$, i.e. completely independent of the weak mixing angle. Technically, the cancellation of the electromagnetic vacuum-polarization effects between charge and photonic field renormalization is due to a Ward identity.

5 Numerical results

For the numerical evaluation we have used the following set of parameters [26]

$$\begin{aligned}
\alpha &= 1/137.0359895, & G_\mu &= 1.166390 \times 10^{-5} \text{ GeV}^{-2}, \\
M_Z &= 91.187 \text{ GeV}, & M_H &= 250 \text{ GeV}, \\
m_e &= 0.51099906 \text{ MeV}, & m_\mu &= 105.65839 \text{ MeV}, & m_\tau &= 1.777 \text{ GeV}, \\
m_u &= 46.0 \text{ MeV}, & m_c &= 1.50 \text{ GeV}, & m_t &= 170 \text{ GeV}, \\
m_d &= 46.0 \text{ MeV}, & m_s &= 150 \text{ MeV}, & m_b &= 4.50 \text{ GeV}.
\end{aligned} \tag{32}$$

The masses of the light quarks are adjusted such that the experimentally measured hadronic vacuum polarization is reproduced [27]. As the Fermi-constant G_μ is empirically much better known than the W mass, M_W is calculated from all the other parameters using the muon decay width including radiative corrections. In this calculation of M_W all parameters given above enter sensibly. If not stated otherwise, M_W is determined in

the following using formulae (2.56) and (2.57) of Ref. [28]. The above set of parameters yields

$$M_W = 80.333 \text{ GeV}.$$

Figure 7 shows the cross-section integrated over the full angular range and the corresponding weak corrections for different polarizations of the incoming photons. In the energy range from threshold up to 1 TeV the weak corrections range between 0 and -10% . For oppositely polarized photons the corrections are about -4% close to threshold and increase smoothly to -8% at 1 TeV. For equally polarized photons the corrections amount to roughly -10% close to threshold, tend to positive values with increasing energy and reach zero at about 1 TeV. The large negative corrections close to threshold originate from top-quark loop corrections to the AAZ^*/χ^* vertices that are enhanced by the large top-quark mass (see Section 4.3). Integrating only over the restricted angular range $20^\circ \leq \theta \leq 160^\circ$ affects the corrections only weakly, as can be seen from Fig. 8.

In Fig. 9 we plot the weak corrections to the differential cross-sections for $\sqrt{s} = 350, 500, 1000 \text{ GeV}$. The angular dependence of the corrections increases with energy. For equally polarized or unpolarized photons the corrections are forward-backward symmetric and take their maximum for $\theta = 90^\circ$. They are usually negative but become positive at high energies in the forward and backward directions. In the case of oppositely polarized photons the corrections are asymmetric with a maximum that moves from the forward or backward direction towards $\theta = 90^\circ$ with increasing energy. This maximum reaches almost -18% at 1 TeV.

In Table 1 we list numerical values for the unpolarized cross-section and the corresponding corrections for several energies and scattering angles. We include the complete corrections corresponding to a soft-photon energy cut-off $\Delta E/E = 0.1$, the QED corrections, the weak corrections and the fermionic and bosonic ones. These numbers show that the fermionic corrections dominate the unpolarized cross-section at low energies. At high energies the fermionic corrections are very small. They are completely absent for oppositely polarized photons. However, in this case the bosonic corrections are large (compare the figures). On the other hand, the bosonic corrections are usually below 1–2% for equally polarized photons.

In Fig. 10 we present the cross-section for equally polarized photons including the weak corrections integrated over $0^\circ < \theta < 100^\circ$ for the Higgs-boson masses $M_H = 350, 400, 500 \text{ GeV}$. Owing to the relatively high threshold for $\gamma\gamma \rightarrow t\bar{t}$ and the large width of such a heavy Higgs boson, the effect of the Higgs resonance is comparably small. In fact a resonance structure is only visible in the range $400 \text{ GeV} \lesssim M_H \lesssim 500 \text{ GeV}$.

Finally, we illustrate in Fig. 11 the M_H -dependence of the integrated cross-section. Outside the Higgs-resonance region the variation is very weak, i.e. below $\sim 1\%$.

6 Summary

The process $\gamma\gamma \rightarrow t\bar{t}$ will allow studies of the properties of the top quark at high-energy photon-photon colliders complementary to the ones achievable by hadron-hadron and electron-positron colliders. In particular, it is useful to investigate the electromagnetic couplings of the top quark.

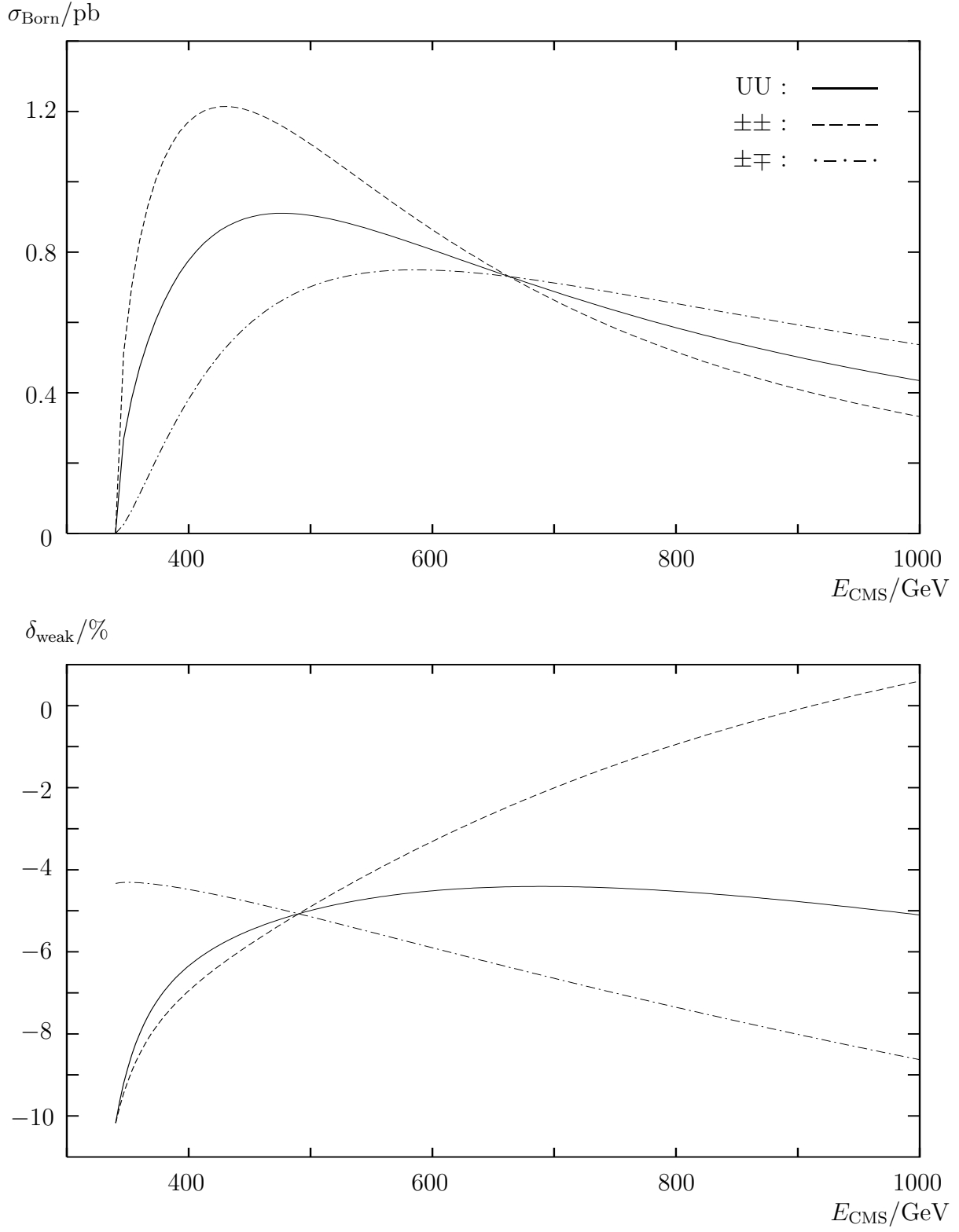


Figure 7: Integrated lowest-order cross-sections and corresponding relative corrections for several polarizations in the full angular range

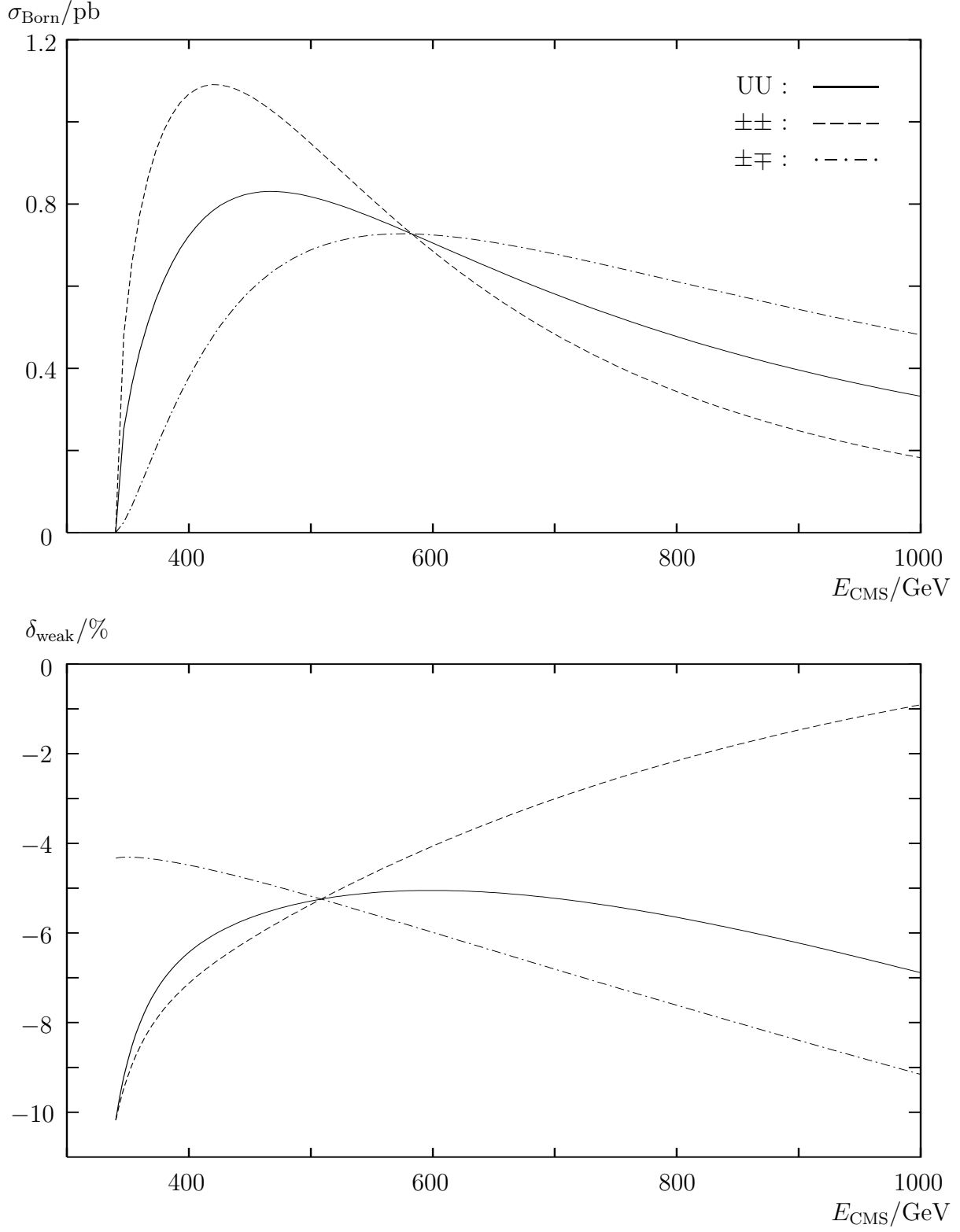


Figure 8: Same as in Fig. 7 but with an angular cut $20^\circ \leq \theta \leq 160^\circ$

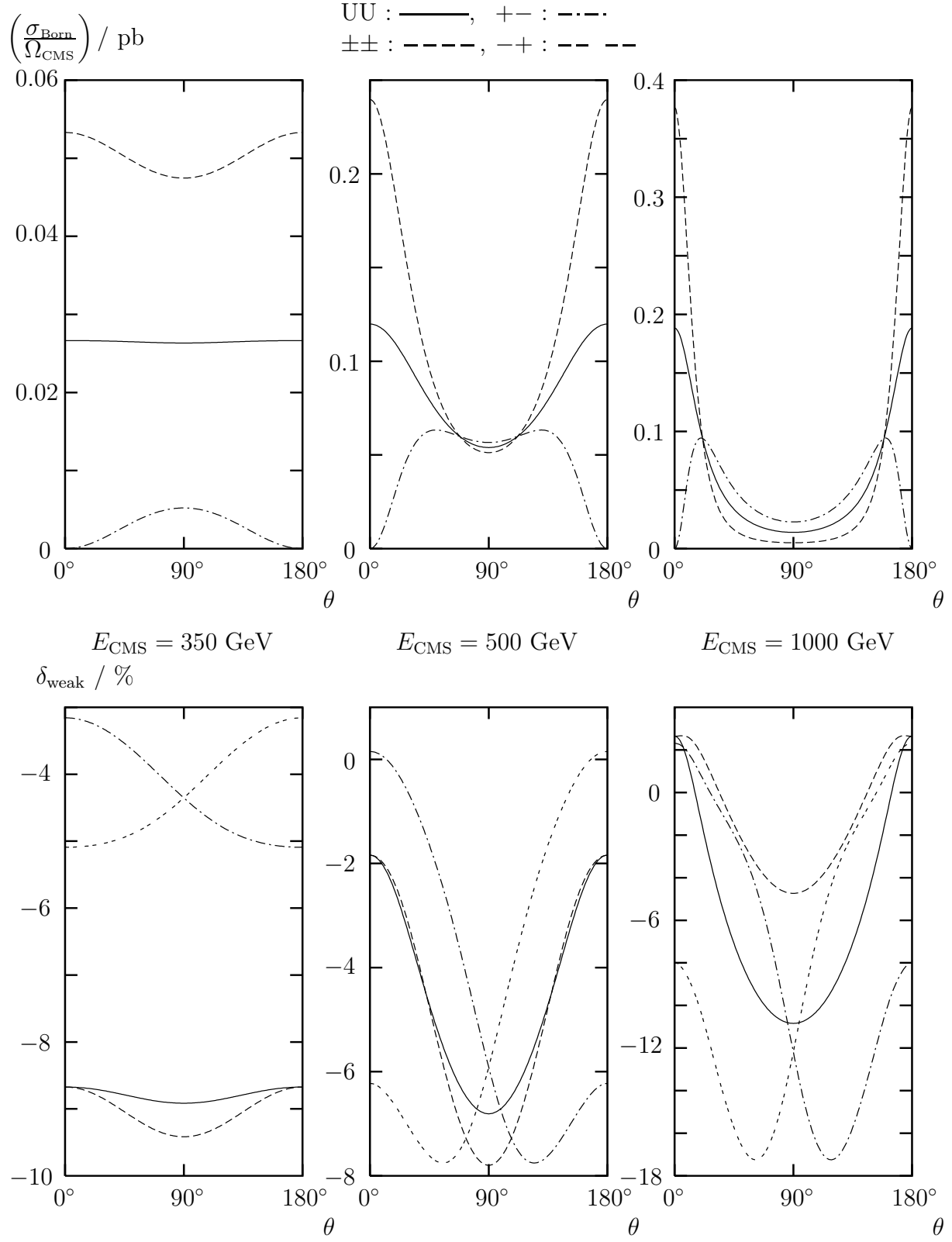


Figure 9: Differential lowest-order cross-sections and relative corrections for the unpolarized cross-section and the cross-sections with equal and unequal photon helicities

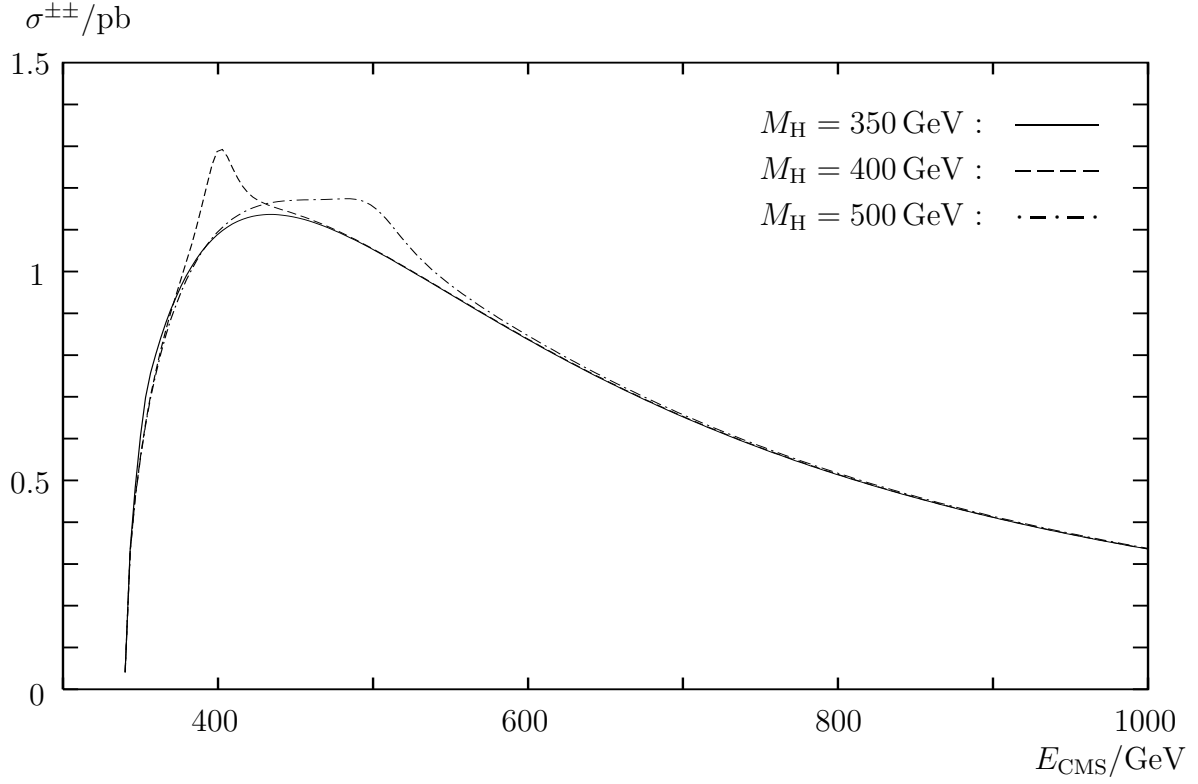


Figure 10: Integrated cross-section ($0^\circ < \theta < 180^\circ$) for equally polarized photons including one-loop corrections for various Higgs masses

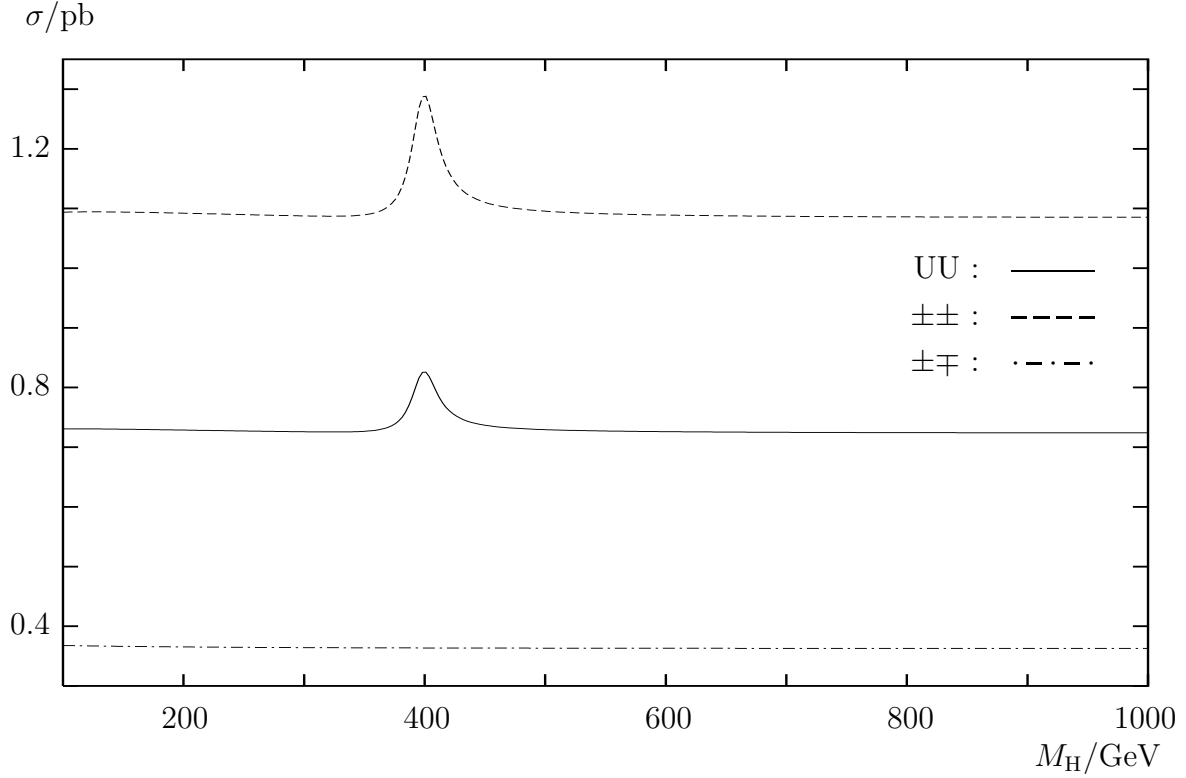


Figure 11: Higgs-mass dependence of the cross-sections in one-loop order for $E_{\text{CMS}} = 400 \text{ GeV}$ ($0^\circ < \theta < 180^\circ$)

E	θ	$\sigma_{\text{Born}}^{\text{UU}}/\text{pb}$	$\delta^{\text{UU}}/\%$	$\delta_{\text{QED}}^{\text{UU}}/\%$	$\delta_{\text{weak}}^{\text{UU}}/\%$	$\delta_{\text{ferm}}^{\text{UU}}/\%$	$\delta_{\text{bos}}^{\text{UU}}/\%$
350 GeV	20°	0.02663	−6.74	1.96	−8.70	−7.86	−0.84
	45°	0.02653	−6.84	1.95	−8.79	−7.72	−1.07
	90°	0.02634	−6.97	1.94	−8.92	−7.55	−1.36
	$20^\circ \leq \theta \leq 160^\circ$	0.31230	−6.89	1.95	−8.84	−7.65	−1.19
	$0^\circ \leq \theta \leq 180^\circ$	0.33248	−6.88	1.95	−8.83	−7.67	−1.17
500 GeV	20°	0.10877	−2.40	0.21	−2.61	−2.97	0.36
	45°	0.07929	−4.53	0.18	−4.71	−2.92	−1.79
	90°	0.05395	−6.66	0.14	−6.81	−3.14	−3.67
	$20^\circ \leq \theta \leq 160^\circ$	0.81785	−5.12	0.17	−5.29	−3.01	−2.28
	$0^\circ \leq \theta \leq 180^\circ$	0.90439	−4.82	0.17	−4.99	−3.01	−1.99
1 TeV	20°	0.09971	−1.75	−0.46	−1.29	0.02	−1.31
	45°	0.03367	−7.66	−0.57	−7.09	0.02	−7.11
	90°	0.01392	−11.48	−0.64	−10.84	0.03	−10.87
	$20^\circ \leq \theta \leq 160^\circ$	0.33208	−7.45	−0.56	−6.89	0.03	−6.91
	$0^\circ \leq \theta \leq 180^\circ$	0.43447	−5.63	−0.53	−5.10	0.03	−5.13

Table 1: Lowest-order cross-sections and relative corrections for unpolarized photons (δ_{QED} is evaluated at $\Delta E = 0.1E$)

We have calculated the complete one-loop virtual and soft-photon radiative corrections to $\gamma\gamma \rightarrow t\bar{t}$ for arbitrarily polarized photons in the electroweak Standard Model. All so-called leading universal corrections – such as the running of the electromagnetic coupling, effects of the ρ -parameter or leading QED logarithms – are absent. However, for equally polarized photons there are large corrections close to the threshold of the process owing to triangle top loops.

We have presented a detailed numerical analysis of the lowest-order cross-sections and the weak radiative corrections. Below 1 TeV the weak corrections are in the range between 0% and −10%. The fermionic corrections vanish for opposite photon polarizations and are otherwise small apart from the triangle top-loop contributions close to threshold. These dominate the corrections at small energies. At high energies, the bosonic corrections dominate in particular for oppositely polarized photons.

Owing to the relatively high threshold the Higgs resonance is not very pronounced. Outside the Higgs-resonance the dependence of the cross-section on the Higgs-boson mass is very weak. In particular, the corrections are finite in the limit of a large Higgs-boson mass.

In summary, our results show that the weak $\mathcal{O}(\alpha)$ corrections to $\gamma\gamma \rightarrow t\bar{t}$ are needed in order to match a per-cent level accuracy. For a complete theoretical prediction QCD, QED and weak corrections as well as finite-width effects of the top quark have to be

combined. Moreover, a convolution with a realistic spectrum for the incoming photons has to be performed.

Appendix

A Interference of SME with the lowest-order matrix element

We list the results for the non-vanishing interference terms (21) for t -channel SME. The corresponding results for the u -channel SME are obtained by the following substitutions

$$\begin{aligned} M^{\lambda_1 \lambda_2, \{V, A\}, u}(i, t) &= M^{\lambda_2 \lambda_1, \{V, A\}, t}(i, u) \Big|_{t \leftrightarrow u}, \\ M^{\lambda_1 \lambda_2, \{V, A\}, u}(i, u) &= M^{\lambda_2 \lambda_1, \{V, A\}, t}(i, t) \Big|_{t \leftrightarrow u}. \end{aligned} \quad (33)$$

Equally polarized photons:

$$\begin{aligned} M^{\pm\pm, V, t}(1, t) &= 8(t - m_t^2)(u - m_t^2)(3m_t^4 - 3m_t^2 t + t^2 - m_t^2 u)/s^2, \\ M^{\pm\pm, V, t}(1, u) &= 8(t - m_t^2)(u - m_t^2)(m_t^4 - tu)/s^2, \\ M^{\pm\pm, V, t}(2, t) &= 4(-2m_t^6 + 2m_t^4 t - m_t^2 t^2 + 4m_t^4 u - 4m_t^2 tu + 2t^2 u - m_t^2 u^2)/s, \\ M^{\pm\pm, V, t}(2, u) &= 4(2m_t^6 - 4m_t^4 t + m_t^2 t^2 - 2m_t^4 u + 4m_t^2 tu + m_t^2 u^2 - 2tu^2)/s, \\ M^{\pm\pm, V, t}(4, t) &= 4(m_t^4 - tu)(-4m_t^4 + 3m_t^2 t - t^2 + m_t^2 u + tu)/s^2, \\ M^{\pm\pm, V, t}(4, u) &= 4(m_t^4 - tu)(-4m_t^4 + m_t^2 t + 3m_t^2 u + tu - u^2)/s^2, \\ M^{\pm\pm, V, t}(6, t) &= 2(m_t^4 - tu)(2m_t^6 - 2m_t^4 t + m_t^2 t^2 - 4m_t^4 u + 4m_t^2 tu - 2t^2 u + m_t^2 u^2)/s^2, \\ M^{\pm\pm, V, t}(6, u) &= 2(m_t^4 - tu)(-2m_t^6 + 4m_t^4 t - m_t^2 t^2 + 2m_t^4 u - 4m_t^2 tu - m_t^2 u^2 + 2tu^2)/s^2, \\ M^{\pm\pm, V, t}(11, t) &= 4m_t^2(2m_t^4 + 2m_t^2 s - s^2 - 4m_t^2 t + 2t^2)/s, \\ M^{\pm\pm, V, t}(11, u) &= 8m_t^2(m_t^4 - tu)/s, \\ M^{\pm\pm, V, t}(12, t) &= 2m_t^2(4m_t^4 - 2m_t^2 t + t^2 + 2m_t^2 u - 4tu - u^2)/s, \\ M^{\pm\pm, V, t}(12, u) &= 2m_t^2(4m_t^4 + 2m_t^2 t - t^2 - 2m_t^2 u - 4tu + u^2)/s, \\ M^{\pm\pm, V, t}(16, t) &= m_t^2(m_t^4 - tu)(-4m_t^4 + 2m_t^2 t - t^2 - 2m_t^2 u + 4tu + u^2)/s^2, \\ M^{\pm\pm, V, t}(16, u) &= m_t^2(m_t^4 - tu)(-4m_t^4 - 2m_t^2 t + t^2 + 2m_t^2 u + 4tu - u^2)/s^2. \end{aligned} \quad (34)$$

All axial SME for equally polarized photons that do not violate CP-invariance vanish after contraction with the Born matrix elements

$$M^{\pm\pm, A, t}(i, j) = 0, \quad i = 1, \dots, 17, \quad j = t, u. \quad (35)$$

Oppositely polarized photons:

$$\begin{aligned} M^{\pm\mp, V, t}(1, t) &= M^{\pm\mp, V, t}(1, u) = M^{\pm\mp, V, t}(4, t) = M^{\pm\mp, V, t}(4, u) \\ &= 4(m_t^4 - tu)(-6m_t^4 + 4m_t^2 t - t^2 + 4m_t^2 u - u^2)/s^2, \\ M^{\pm\mp, V, t}(6, t) &= M^{\pm\mp, V, t}(6, u) = 2(t - u)(m_t^4 - tu)^2/s^2, \\ M^{\pm\mp, V, t}(14, t) &= M^{\pm\mp, V, t}(14, u) = 4m_t^2(m_t^4 - tu), \\ M^{\pm\mp, V, t}(16, t) &= M^{\pm\mp, V, t}(16, u) = -4m_t^2(m_t^4 - tu)^2/s^2, \\ M^{\pm\mp, A, t}(1, t) &= M^{\pm\mp, A, t}(1, u) = M^{\pm\mp, A, t}(4, t) = M^{\pm\mp, A, t}(4, u) \end{aligned}$$

$$\begin{aligned}
&= \mp 4(t-u)(m_t^4 - tu)/s, \\
M^{\pm\mp, A, t}(6, t) &= M^{\pm\mp, A, t}(6, u) = \pm 2(m_t^4 - tu)^2/s, \\
M^{\pm\mp, A, t}(14, t) &= M^{\pm\mp, A, t}(14, u) = \pm 4m_t^2(m_t^4 - tu).
\end{aligned} \tag{36}$$

References

- [1] F. Abe et al., CDF collaboration, FERMILAB-PUB-95/022-E, hep-ex/9503002.
- [2] S. Abachi et al., DØ collaboration, FERMILAB-PUB-95/028-E, hep-ex/9503003.
- [3] The LEP collaborations and the LEP Electroweak Working Group, CERN/PPE/94-187; contributed to the 27th International Conference on High-Energy Physics - ICHEP 94, Glasgow, Scotland, UK, 20 - 27 Jul 1994.
- [4] W. Bernreuther et al., in *e⁺e⁻ Collisions at 500 GeV: The Physics Potential*, ed. P.M. Zerwas (DESY 92-123A, Hamburg, 1992), p. 255.
- [5] I.F. Ginzburg, G.L. Kotkin, V.G. Serbo and V.I. Telnov, *Nucl. Instr. Meth.* **205** (1983) 47;
I.F. Ginzburg, G.L. Kotkin, S.L. Panfil, V.G. Serbo and V.I. Telnov, *Nucl. Instr. Meth.* **219** (1984) 5;
V.I. Telnov, *Nucl. Instr. Meth.* **A294** (1990) 72.
- [6] S.J. Brodsky, P.M. Zerwas, *Nucl. Instr. Meth.* **A355** (1995) 19.
- [7] O.J.P. Éboli, M.C. Gonzalez-Garcia, F. Halzen and S.F. Novaes, *Phys. Rev.* **D47** (1993) 1889;
I.I. Bigi, F. Gabbiani and V.A. Khoze, *Nucl. Phys.* **B406** (1993) 3;
K. Fujii, T. Matsui and Y. Sumino, *Phys. Rev.* **D50** (1994) 4341.
- [8] S.Y. Choi and K. Hagiwara, preprint KEK-TH-443, hep-ph/9506430.
- [9] J.H. Kühn, E. Mirkes and J. Steegborn, *Z. Phys.* **C57** (1993) 615;
M. Drees, M. Krämer, J. Zunft and P.M. Zerwas, *Phys. Lett.* **B306** (1993) 371;
B. Kamal, Z. Merebashvili and A.P. Contogouris, *Phys. Rev.* **D51** (1995) 4808.
- [10] S. Moretti, DFTT 39/95, DTP/95/56, hep-ph/9506466.
- [11] E. Boos, I. Ginzburg, K. Melnikov, T. Sack and S. Shichanin, *Z. Phys.* **C56** (1992) 487.
- [12] H. Veltman, *Z. Phys.* **C62** (1994) 235.
- [13] S. Wolfram, *Mathematica — A System for Doing Mathematics by Computer* (Addison-Wesley, Redwood City, CA, 1988).
- [14] J. Küblbeck, M. Böhm and A. Denner, *Comp. Phys. Commun.* **60** (1990) 165;
H. Eck and J. Küblbeck, *Guide to FeynArts 1.0*, University of Würzburg, 1992.
- [15] R. Mertig, M. Böhm and A. Denner, *Comp. Phys. Commun.* **64** (1991) 345;
R. Mertig, *Guide to FeynCalc 1.0*, University of Würzburg, 1992.

- [16] W. Beenakker, A. Denner, W. Hollik, R. Mertig, T. Sack and D. Wackeroth, *Nucl. Phys.* **B411** (1994) 343.
- [17] A. Denner, *Fortschr. Phys.* **41** (1993) 307.
- [18] G. Passarino and M. Veltman, *Nucl. Phys.* **B160** (1979) 151.
- [19] G. 't Hooft and M. Veltman, *Nucl. Phys.* **B153** (1979) 365;
W. Beenakker and A. Denner, *Nucl. Phys.* **B338** (1990) 349;
A. Denner, U. Nierste and R. Scharf, *Nucl. Phys.* **B367** (1991) 637.
- [20] G.J. van Oldenborgh, *Comp. Phys. Commun.* **66** (1991) 1.
- [21] T. Appelquist and C. Bernard, *Phys. Rev.* **D22** (1980) 200;
A.C. Longhitano, *Nucl. Phys.* **B188** (1981) 118.
- [22] A. Denner, S. Dittmaier and R. Schuster, *Phys. Rev.* **D51** (1995) 4738; Bielefeld preprint BI-TP 95/04, Würzburg preprint WUE-ITP-95-002, hep-ph/9503442, to appear in *Nucl. Phys.* **B**.
- [23] E. Braaten and J.P. Leveille, *Phys. Rev.* **D22** (1980) 715;
M. Drees and K. Hikasa, *Phys. Lett.* **B240** (1990) 455, *E:Phys. Lett.* **B262** (1991) 497;
J. Fleischer and F. Jegerlehner, *Phys. Rev.* **D23** (1981) 2001;
D.Yu. Bardin, P.Kh. Khristova and B.M. Vilenskii, *Sov. J. Nucl. Phys.* **53** (1991) 152 and Dubna preprint JINR-P2-91-140;
B.A. Kniehl, *Nucl. Phys.* **B352** (1991) 1, *Nucl. Phys.* **357** (1991) 439 and *Nucl. Phys.* **376** (1992) 3;
A. Dabelstein and W. Hollik, *Z. Phys.* **C53** (1992) 507.
- [24] V.S. Fadin and V.A. Khoze, *JETP Lett.* **46** (1987) 525; *Sov. J. Nucl. Phys.* **48** (1988) 309; **53** (1991) 692.
- [25] S. Dittmaier and C. Grosse-Knetter, Bielefeld preprint BI-TP 95/10, hep-ph/9505266.
- [26] Particle Data Group, *Phys. Rev.* **D50** (1994) 1173.
- [27] M.L. Swartz, preprint SLAC-PUB-6710, 1994, hep-ph/9411353;
A.D. Martin and D. Zeppenfeld, *Phys. Lett.* **B345** (1995) 558;
S. Eidelman and F. Jegerlehner, preprint PSI-PR-95-01, BudkerINP 95-5, hep-ph/9502298;
H. Burkhardt and B. Pietrzyk, preprint LAPP-EXP-95.05.
- [28] W. Beenakker and A. Denner, *Int. J. Mod. Phys.* **A9** (1994) 4837.